Sensors and Materials, Vol. 32, No. 7 (2020) 2399–2408
MYU Tokyo

S & M 2268

Optoelectronic Characteristics of rr-P3HT:PC61BM-based Organic Solar Cells

Jean Pierre Ndabakuranye,[1] Hyeonju Lee,[1] Idrissa Kayijuka,[2]
Sungkeun Baang,[1,3*] and Jaehoon Park[1,3**]

[1]Department of Electronic Engineering, Hallym University, 1 Hallymdaehak-gil, Chuncheon 24252, South Korea
[2]Department of Mathematics, Ege University, Kampüsü, Izmir 35040, Turkey
[3]School of Software, Hallym University, 1 Hallymdaehak-gil, Chuncheon 24252, South Korea

(Received September 1, 2019; accepted April 29, 2020)

Keywords: rr-P3HT, PC61BM, solar cells

It is well known that organic solar cells (OSCs) are made using organic materials because of their mechanical flexibility and low manufacturing cost. Their efficiency, however, remains low for several reasons, including limited light absorption and poor charge mobility. Although OSCs are a fascinating supplement to silicon-based solar cells, they have yet to provide good efficiency for a prolonged period. Combining a narrowband donor and an electron acceptor [regioregular poly 3-hexylthiohene-2,5-diyl (rr-P3HT) and 6,6-phenyl-C61-butyric acid methyl ester (PC61BM), respectively] is a prevalent approach towards efficient organic cells. In our work, a device of configuration indium tin oxide (ITO)/poly(3,4-ethylenedioxythiophene):polystyrene sulfonate (PEDOT:PSS)/rr-P3HT:PC61BM/Al was fabricated and characterized both electrically and optically. Various solar cell constraints were optimized to maximize the performance of OSCs. Ultimately, a device with a maximum power conversion efficiency (PCE) of approximately 1.4% was achieved under the optimum fabrication conditions.

1. Introduction

The idea of organic solar cells (OSCs) may seem strange because organic materials are inherently insulators, but they can be converted into semiconductors if charge carriers are generated by injection, optical excitation, and doping.[1–3] In fact, devices such as organic thin-film transistors made from conjugated polymers date back to the 1980s.[3] The electronic structure of organic semiconductors is rather unusual: (i) π-bonds between carbon atoms form the highest occupied molecular orbital (HOMO) and lowest unoccupied molecular orbital (LUMO). (ii) Light absorption does not result in the generation of electron–hole pairs (EHPs), but rather in excited states–excitons.[4,5] These states are localized and surrounded by significant nuclear relaxation,[6,7] and the energy keeping the exciton intact is known as the binding energy (E_B) as follows:

*Corresponding author: e-mail: baang@hallym.ac.kr
**Corresponding author: e-mail: jaypark@hallym.ac.kr
https://doi.org/10.18494/SAM.2020.2807

$$E_B = \frac{e^2}{4\pi\varepsilon_o\varepsilon_r r_c}. \quad (1)$$

In this case, an exciton will dissociate when $E_B \leq k_B T$ at room temperature, as in Eq. (2). Here, k_B is the Boltzmann constant and r_c is the critical distance between opposite charge carriers in an exciton in a molecular material.[3] In molecular solids, because the dielectric constant is low (approximately 3−4), the optical absorption normally generates an excitonic state with a binding energy of 0.5 to 1 eV.[2] In this case, the combination of two materials with the proper chemical potential offset results in exciton dissociation and, hence, the feasibility of OSCs.

$$r_c \geq \frac{e^2}{4\pi\varepsilon_o\varepsilon_r k_B T} \quad (2)$$

OSCs are attractive because of their light weight, large-area feasibility, mechanical flexibility, and easy manufacturing through solution processing.[8–10] They present various inherent advantages such as ultrafast optoelectronic response and chemical tenability through molecular design.[11–13] OSCs are envisaged to open up new fields of application in disposable sensors because they can supply the power for small mobile devices. It is possible to combine OSCs with low-end sensors and electronic circuits on a small strip of plastic to form self-powered sensing systems. However, because of their narrow absorption spectra and poor charge mobility, their efficiency remains low compared with their Si-based counterparts.[13–15] Among all the scientific reports, those on P3HT:PCBM bulk heterojunction (BHJ)-based solar cells are the most promising.[9,16] This is due to the semicrystalline structure of regioregular poly 3-hexylthiohene-2,5-diyl (rr-P3HT) (in the polythiophene family), the high hole mobility of 6,6-phenyl-C61-butyric acid methyl ester (PC61BM) (among the fullerene derivatives), and the BHJ structure that improves both charge photogeneration and transport through donor−acceptor combination into a single active layer.[16,17]

In this study, cells of indium tin oxide (ITO)/poly(3,4-ethylenedioxythiophene):polystyrene sulfonate (PEDOT:PSS)/rr-P3HT:PC61BM/Al configuration were fabricated and characterized. Various parameters were optimized to enhance the device performance. Furthermore, because a suitable solvent enhances both charge generation and charge transfer to the electrodes,[13,18] dichlorobenzene (DCB) was used as a solvent, as it provides good phase separation and aids the self-alignment of rr-P3HT chains, hence improving its crystal structure and ultimately its power conversion efficiency (PCE).

2. Materials and Methods

2.1 Materials

rr-P3HT was purchased from Aldrich and used as supplied, and 1,2-DCB ($C_6H_4Cl_2$, Junsei, Mw: 147.0 g/mol, ≥99%) was used as supplied. Furthermore, PC61BM (99.5%) was used as

supplied, and PEDOT:PSS (1.3 wt% dispersion in H_2O) was purchased from Sigma-Aldrich. The chemical structures of rr-P3HT and PC61BM are shown in Fig. 1. Solar cells were fabricated on indium tin oxide (ITO) substrates. The substrates were used as supplied. Aluminum pellets (iNexusinc, 99.999%) were used for electrode deposition as supplied. Acetone (CH_3COCH_3, Samchun Pure Chemical, Mw: 58.08 g/mol, ≥99.7%), isopropanol [$(CH_3)_2CHOH$, Samchun Pure Chemical, Mw: 60.10 g/mol, ≥99.5%], and deionized water (18.2 MΩ·cm) were used for ultrasonication cleaning of the substrate.

2.2 Material preparation

For all our experiments, PEDOT:PSS was stirred for 30 min before being used. Subsequently, rr-P3HT and PC61BM were mixed in a 1:1 ratio and dissolved in DCB to form a solution with a concentration of 20 mg/mL. The solution was stirred for 12 h (overnight) at 1500 rpm and at 40 °C in nitrogen.

2.3 Cleaning

ITO-patterned substrates (2.5 × 2.5 cm^2) and vials (solution bottles) were dipped in acetone and sonicated for 15 min, then in isopropanol and sonicated for 15 min, and finally in deionized water and sonicated for 15 min. The substrates and the vials were blow-dried with nitrogen and then kept in an oven for gentle drying, away from air turbulence and possible contaminants. Before processing, the substrates underwent UV-ozone surface treatment for 15 min.

2.4 Cell fabrication

The systematic device fabrication procedure is shown in Fig. 2. The surface-treated ITO-patterned glass substrate was placed on top of the vacuum spin chuck of a spin coater, which was then switched to vacuum. The PEDOT:PSS solution was filtered using a PVDF filter (pore size: 0.45 μm), spin-coated onto an ITO substrate for 48 s, and then annealed at 150 °C for 10 min. After a few seconds off the hot plate, the PEDOT:PSS-coated substrate was placed

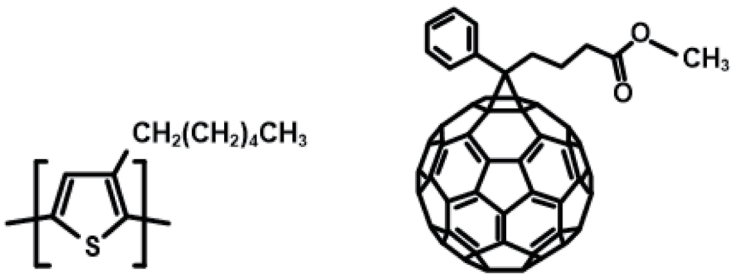

(a) (b)

Fig. 1. Chemical structures of (a) rr-P3HT and (b) PC61BM.

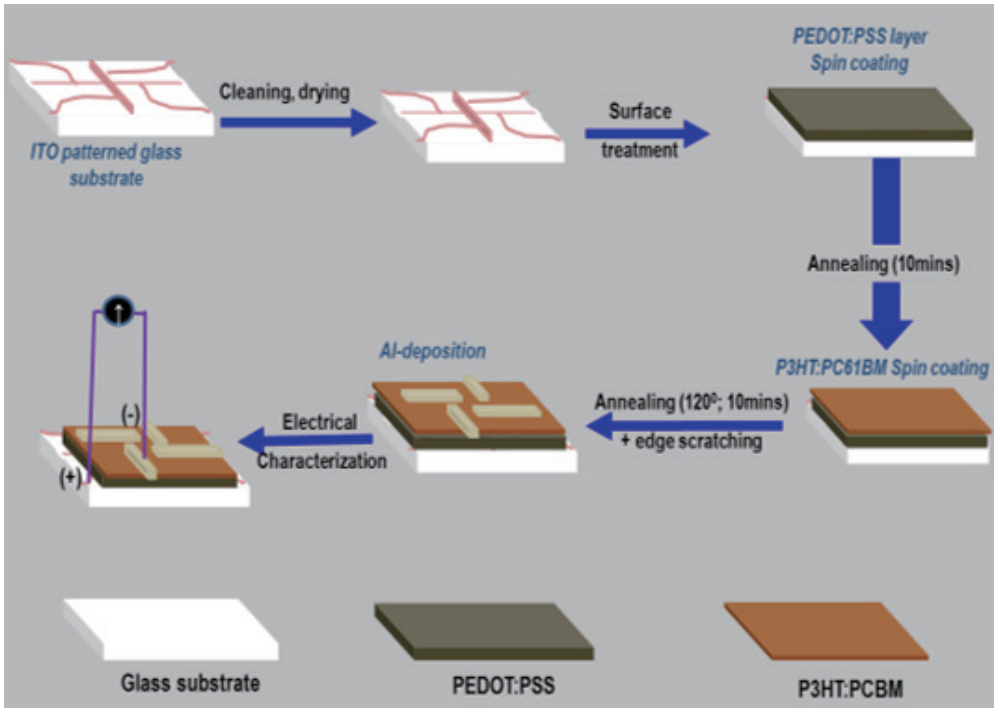

Fig. 2. (Color online) Device fabrication steps.

back onto the vacuum spin chuck. The prepared rr-P3HT:PC61BM solution was filtered with a PTFE filter (pore size: 0.45 μm), spin-coated on top of the PEDOT:PSS layer for 48 s, and then annealed at 120 °C for 10 min. Next, a triangular cotton swab was used to erase an area at the substrate edges before aluminum electrode deposition. The substrate was placed onto a shadow mask and put in a thermal evaporation system, aluminum pellets were loaded onto a tungsten boat, and then the deposition system was pumped down to low vacuum (approximately 5×10^{-3} Torr) and later to high vacuum (approximately 10^{-6} Torr) prior to deposition. After deposition, the chamber was allowed to return to atmospheric pressure during substrate cooling. The substrate was finally taken out of the chamber for electrical and optical characterizations.

2.5 Cell characterization

The *I–V* characterization was begun immediately to avoid any delays that would result in device degradation. Characterization was done using a solar simulator. The following solar-cell parameters were determined: open-circuit voltage (V_{OC}), short-circuit current (I_{SC}), maximum power (P_{max}), PCE, shunt resistance (R_{sh}), series resistance (R_s), and fill factor (FF). To characterize every cell on each substrate, an eight-terminal pinned jig was used to hold the substrate tight. The jig with the substrate was placed inside the solar simulator and was then irradiated with light that mimicked the solar spectrum (air mass 1.5). This took place in a dark system to avoid light shielding.

2.6 Thermal annealing

Various reports claim that thermal treatment improves the solar cell PCE.[19,20] After a range of tests, the most favorable annealing temperatures were found. The optimal temperatures used in this study were 120 °C for rr-P3HT:PC61BM and 150 °C for PEDOT:PSS. Annealing was used after spin coating to evaporate some of the solvent residue in the material, as well as to vary the morphology of the material that had just been spin-coated. In our experiments, post-annealing treatment (annealing after aluminum deposition) was not required because it decreased the PCE values of OSCs.

3. Results and Discussion

PEDOT:PSS and rr-P3HT:PC61BM films were spin-coated on glass substrates. The transmittance spectra were obtained. UV–vis spectra of the PEDOT:PSS (annealed at 120 °C for 10 min) and rr-P3HT:PC61BM (annealed at 150 °C for 10 min) films were obtained to observe the absorption profiles for both materials under various dispositions (Fig. 3). In this experiment, the spinning speed for the spin-coating process was varied. Clearly, PEDOT:PSS exhibits weak absorption spectra, as shown in Fig. 3(a). This is beneficial because the purpose of PEDOT:PSS is not to absorb photons but to act as a hole-transport layer.[21] However, the rr-P3HT:PC61BM blend exhibits absorption peaks in the 330−650 nm region, as shown in Fig. 3(b). The shoulders in the absorption profiles indicate the crystallinity in the rr-P3HT:PC61BM film, especially the pronounced vibronic shoulders at approximately 560 nm and approximately 610 nm, which are attributed to the increased planarity of rr-P3HT backbones, coupling between C=C stretching and the π−to−π* electronic transition.[22] The absorption of films was weak at increased spin coating speeds. Also, rr-P3HT:PC61BM showed increased absorbance between 400 and 600 nm; this was possibly caused by the wide absorption band of P3HT.[23] After optical

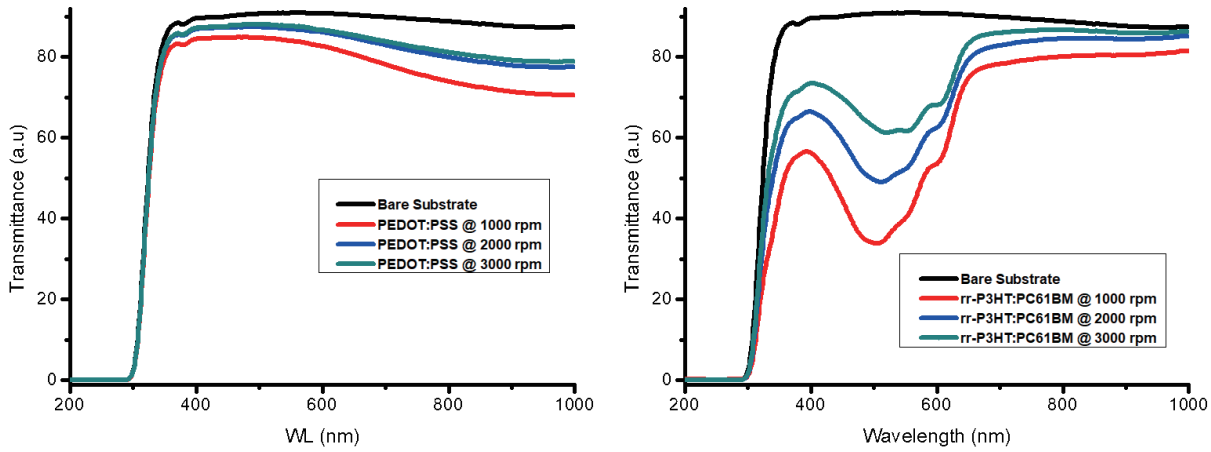

(a) (b)

Fig. 3. (Color online) Optical transmittance of thin film materials. (a) PEDOT:PSS. (b) rr-P3HT:PC61BM.

measurements, the thickness of each film was measured and the results are summarized in Table 1. The results show that the higher the spin-coating speed, the thinner the film and ultimately the lower the absorbance.

The *I–V* characterization was accomplished using a solar simulator. The PCE for the four cells on each substrate was measured by switching the contacts. However, at first, there was a difficulty in realizing the functionality of cells because of two issues: (1) the roughness of the surface of the substrate and (2) the difficulty in making contacts between the jig pins and the electrodes. These issues were solved by (1) wetting the surface of the substrate through surface treatment and (2) adequate erasing of the edges of the substrate before aluminum deposition. The distribution of the initial PCE values for all 96 OSCs is shown in Fig. 4. The PCE for all the manufactured cells ranged from 0 to 1.4%. After post-annealing treatment, the PCE of the device with the highest PCE was degraded from 0.69 to 0.08%, which is equivalent to a decrease of approximately 90%. During the study, devices were manufactured under what were called "dispositions" based on the spin-coating speeds in rpm for PEDOT:PSS and rr-P3HT:PC61BM films (see Table 2). Here, considering the 1.4% PCE of the Deposition II OSC case, an A4-sheet-sized module fabricated through the Deposition II condition will supply an electronic power of approximately 831.6 mW for portable sensor systems, which is sufficient for typical temperature sensors with a power consumption of 800 mW.

The *I–V* curves for high-performing cells in each disposition are compared in Fig. 5. Dispositions IV, V, VI, X, XI, and XII are absent because they gave low to zero PCE. The highest performance in our experiments was found for Disposition II, under which the main spin-coating speeds of PEDOT:PSS and rr-P3HT:PC61BM were 2000 and 500 rpm,

Table 1
Thickness results for rr-P3HT:PC61BM and PEDOT:PSS.

	1000 rpm	2000 rpm	3000 rpm
rr-P3HT:PC61BM	55 nm	40 nm	30 nm
PEDOT:PSS	100 nm	70 nm	35 nm

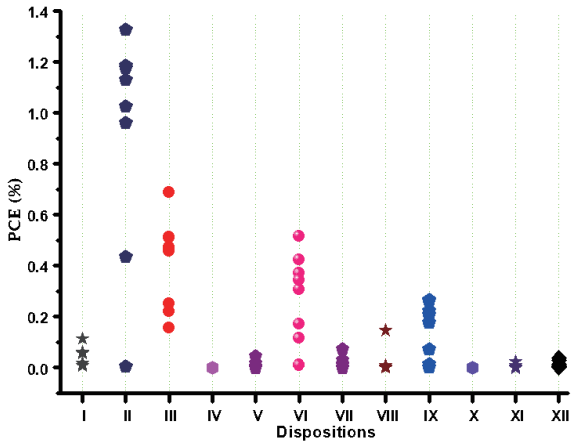

Fig. 4. (Color online) Initial PCE distribution (96 PCEs).

Table 2
Fabrication dispositions.

	PEDOT:PSS	rr-P3HT:PC61BM
Disposition I	1000	500
Disposition II	2000	500
Disposition III	3000	500
Disposition IV	1000	1000
Disposition V	2000	1000
Disposition VI	3000	1000
Disposition VII	1000	2000
Disposition VIII	2000	2000
Disposition IX	3000	2000
Disposition X	1000	3000
Disposition XI	2000	3000
Disposition XII	3000	3000

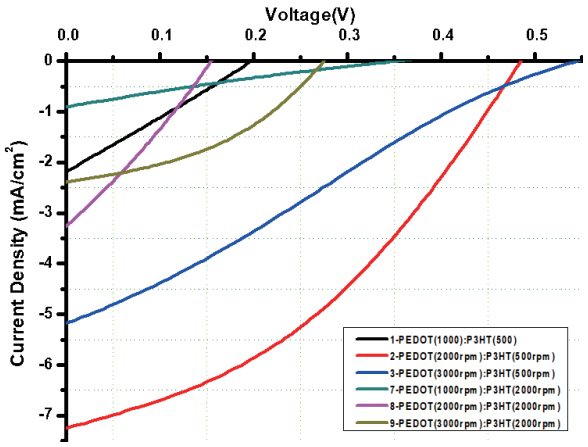

Fig. 5. (Color online) *I–V* curves of high-performing cells within each disposition.

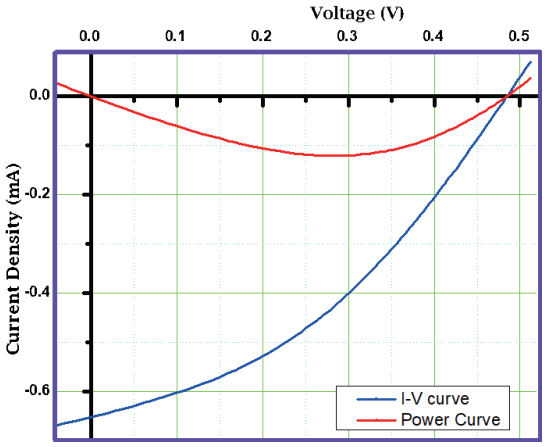

Fig. 6. (Color online) *I–V* (blue) and power (red) curves for the solar cell with the highest PCE in this study.

respectively. The values of all PCEs obtained ranged from 0 to 1.4%, and Disposition II [PEDOT:PSS(2000 rpm)/rr-P3HT:PC61BM(500 rpm)] gave the highest set of efficiencies of all dispositions. The *I–V* characteristics of the device with the highest PCE are shown in Fig. 6.

These high efficiencies obtained in Disposition II can be attributed to (1) the increased thickness of rr-P3HT:PC61BM caused by the low spin-coating speed (see Table 2), which enhances the light absorption, hence the increased current density (for comparison with other dispositions, see Fig. 5), and (2) the higher spin-coating speed resulting in the reduced thickness of PEDOT:PSS. This ensures the transmission of most of the photons and also the uniform distribution of the material on the substrate, which enhance the hole collection at the electrodes. Both of these factors ultimately resulted in increased current density. At a lower spin-coating speed, the distribution of rr-P3HT:PC61BM on top of PEDOT:PSS was uneven. The distribution became more uneven at a lower spin-coating speed of PEDOT:PSS.

Regarding the increased PCE, it has been accepted only recently that the origin of the open-circuit voltage V_{oc} for BHJ OSCs is the splitting of the electrochemical potentials of holes and electrons determined by their fermionic nature.[24,25] Here, the increased V_{oc} enhanced the PCE because of the generation of a greater amount of polarons at the rr-P3HT/PC61BM interface through charge separation. Figure 6 shows that the power generated by the highest performance was low. Although this solar cell exhibited the highest performance among the cells in this study, the PCE was clearly low. This could be attributed to high series resistance (see Table 3), and this might imply the presence of charge carrier traps (recombination sites) in the fabric of the active layer.

Cells under Dispositions VI and VII were further characterized after 10 min of post-annealing at 120 °C. Unfortunately, the post-annealing treatment reduced the PCE, and the *I–V* characteristics before and after post-annealing treatment are compared in Fig. 7. The PCE for the best-performing cells in Dispositions VI and VII decreased, respectively, from 0.688 to 0.076% (~90% decrease) and from 0.517 to 0.3832% (~26% decrease). This degradation

Table 3
Parameters for the solar cell with best performance.

Disposition	V_{oc} (V)	J_{sc} (mA/cm^2)	P_{max} (mW)	FF (%)	PCE (%)	R_{sh} (kΩ)	R_s (kΩ)
PEDOT:PSS(2000)/ rr-P3HT:PC61BM(500)	0.48	7.24	0.12	37.84	1.43	1.82	0.41

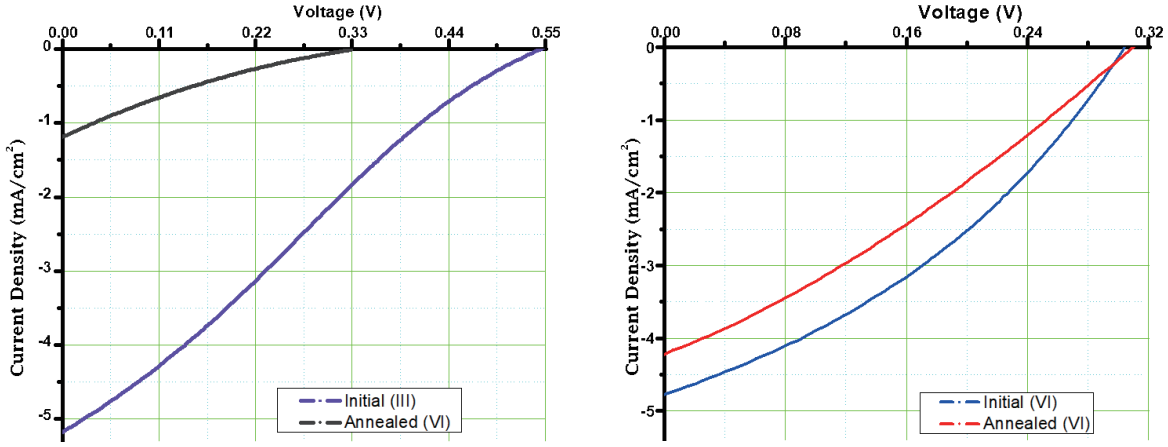

(a) (b)

Fig. 7. (Color online) *I–V* curves obtained (a) before and (b) after annealing.

in device performance with thermal treatment is attributed to (1) the thermally induced domain growth (hence, the possibility of unfavourable phase separation between rr-P3HT and PC61BM),[23,26–29] and (2) the possible deterioration of the electrical contact between the organic layer and aluminum electrode, which implies hindered charge transport and increased recombination,[28,29] resulting in the apparent reduction in short-circuit current. The poor thermal stability of the present OSCs may allow the low-temperature operation of electronic devices. Therefore, the thermal stability of solution-processed OSCs should be taken into account when determining the operation temperature of embedded sensor systems.

4. Conclusion

Although OSCs are projected as low-cost and facile processable solar cells, their PCE with small-area cells is still low, and it is necessary to realize a PCE of at least 15% for their commercialization in widespread applications. In the present study, we fabricated OSCs with the configuration of ITO/PEDOT:PSS/rr-P3HT:PC61BM/Al and analyzed their electrical characteristics. The cells' efficiencies under various spin-coating speeds and annealing treatment temperatures were examined. For all the fabricated substrates, the PCE varied from 0 to 1.4%. By varying the spin-coating speed, the film thickness changes, and this results in the variation of the performance of the fabricated OSCs. Additionally, it is found that post-annealing of the fabricated OSCs is detrimental to the adhesion characteristics among

rr-P3HT and PC61BM molecules and also deteriorates the electrical contact at the organic semiconductor/metal electrode interface. This ultimately degrades the OSC performance. We believe that the results constitute a basis for optimizing the fabrication process of solution-processed OSCs. This study can be extended to develop self-powered sensor systems in which OSCs are embedded to supply electrical power. Further research should be conducted on the effect of thermal treatment on the interfacial characteristics between the organic semiconductor layer and electrodes in solution-processed OSCs.

Acknowledgments

This research was supported by the Hallym University Research Fund, 2019 (HRF-201907-016).

References

1 Y.-J. Hsiao, T.-H. Fang, L.-W. Ji, Y.-C. Lee, and B.-T. Dai: Electrochem. Commun. **18** (2012) 4. https://doi.org/10.1016/j.elecom.2012.01.030
2 L. Wang and D. Beljonne: J. Chem. Phys. **139** (2013) 064316. https://doi.org/10.1063/1.4817856
3 M. Wang, P. Baek, A. Akbarinejad, D. Barker, and J. Travas-Sejdic: J. Mater. Chem. C **19** (2019) 5534. https://doi.org/10.1039/C9TC00709A
4 B. Schweitzer and H. Bässler: Synth. Met. **109** (2000) 1. https://doi.org/10.1016/S0379-6779(99)00187-3
5 O. Inganäs: Adv. Mater. **30** (2018) 1800388. https://doi.org/10.1002/adma.201800388
6 U. Bockelmann: Phys. Rev. B **48** (1993) 17637. https://doi.org/10.1103/PhysRevB.48.17637
7 N. Banerji, S. Cowan, M. Leclerc, E. Vauthery, and A. J. Heeger: J. Am. Chem. Soc. **132** (2010) 17459. https://doi.org/10.1021/ja105290e
8 F. C. Krebs: Sol. Energy Mater. Sol. Cells **93** (2009) 394. https://doi.org/10.1016/j.solmat.2008.10.004
9 M. T. Dang, L. Hirsch, and G. Wantz: Adv. Mater. **23** (2011) 3597. https://doi.org/10.1002/adma.201100792
10 B. O'Regan and M. Grätzel: Nature **353** (1991) 737. https://doi.org/10.1038/353737a0
11 E. A. Lukina, A. A. Popov, M. N. Uvarov, and L. V. Kulik: J. Phys. Chem. B **119** (2015) 13543. https://doi.org/10.1021/acs.jpcb.5b02142
12 S. N. Clafton, D. M. Huang, W. R. Massey, and T. W. Kee: J. Phys. Chem. B **117** (2013) 4626. https://doi.org/10.1021/jp308876z
13 S. Günes, H. Neugebauer, and N. S. Sariciftci: Chem. Rev. **107** (2007) 1324. https://doi.org/10.1021/cr050149z
14 S. E. Shaheen, C. J. Brabec, and N. S. Sariciftci: Appl. Phys. Lett. **78** (2001) 841. https://doi.org/10.1063/1.1345834
15 J. Wang, S. Xie, D. Zhang, R. Wang, Z. Zheng, H. Zhou, and Y. Zhang: J. Mater. Chem. A **6** (2018) 19934. https://doi.org/10.1039/C8TA07954D
16 S. Dong, K. Zhang, B. Xie, J. Xiao, H.-L. Yip, H. Yan, F. Huang, and Y. Cao: Adv. Energy Mater. **9** (2019) 1802832. https://doi.org/10.1002/aenm.201802832
17 D. Chen, A. Nakahara, D. Wei, D. Nordlund, and T. P. Russell: Nano Lett. **11** (2011) 561. https://doi.org/10.1021/nl103482n
18 I. Deckman, M. Moshonov, S. Obuchovsky, R. Brener, and G. Frey: J. Mater. Chem. A **2** (2014) 16746. https://doi.org/10.1039/C4TA03912B
19 W. Wang, S. Pröller, M. A. Niedermeier, V. Körstgens, M. Philipp, B. Su, D. M. González, S. Yu, S. V. Roth, and P. Müller-Buschbaum: ACS Appl. Mater. Interfaces **7** (2015) 602. https://doi.org/10.1021/am5067749
20 T. Oku, S. Hori, A. Suzuki, T. Akiyama, and Y. Yamasaki: Jpn. J. Appl. Phys. **53** (2014) 05FJ08. https://doi.org/10.7567/JJAP.53.05FJ08
21 D. Wakizaka, T. Fushimi, H. Ohkita, and S. Ito: Polymer **45** (2004) 8561. https://doi.org/10.1016/j.polymer.2004.10.007
22 E. Ishow, G. Clavier, F. Miomandre, M. Rebarz, G. Buntinx, and O. Poizat: Phys. Chem. Chem. Phys. **15** (2013) 13922. https://doi.org/10.1039/C3CP51480C
23 Y.-T. Wang, M.-H. Chen, C.-T. Lin, J.-J. Fang, C.-J. Chang, C.-W. Luo, A. Yabushita, K.-H. Wu, and T. Kobayashi: ACS Appl. Mater. Interfaces **7** (2015) 4457. https://doi.org/10.1021/am508091u

24 G. Garcia-Belmonte and J. Bisquert: Appl. phys. Lett. **96** (2010) 113301. https://doi.org/10.1063/1.3358121
25 O. Ostroverkhova: Chem. Rev. **116** (2016) 13279. https://doi.org/10.1021/acs.chemrev.6b00127
26 A. J. Parnell, A. J. Cadby, O. O. Mykhaylyk, A. D. F. Dunbar, P. E. Hopkinson, A. M. Donald, and R. A. L. Jones: Macromolecules **44** (2011) 6503. https://doi.org/10.1021/ma2007706
27 R. Kang, S.-H. Oh, S.-I. Na, T.-S. Kim, and D.-Y. Kim: Sol. Energy Mater. Sol. Cells **120** (2014) 131. https://doi.org/10.1016/j.solmat.2013.08.026
28 Z. Zhao, L. Rice, H. Efstathiadis, and P. Haldar: Microelectron. Reliab. **53** (2013) 123. https://doi.org/10.1016/j.microrel.2012.08.002
29 B. Ray, P. R. Nair, and M. A. Alam: Sol. Energy Mater. Sol. Cells **95** (2011) 3287. https://doi.org/10.1016/j.solmat.2011.07.006